DE GRUYTER OPEN
Studia Geotechnica et Mechanica, Vol. 38, No. 1, 2016
DOI: 10.1515/sgem-2016-0013

TECHNICAL NOTE

LIQUEFACTION MECHANISM INDUCED BY DYNAMIC EXCITATION MODELED IN PLAXIS AE WITH THE USE OF UBC AND MOHR–COULOMB CONSTITUTIVE RELATIONSHIPS

ANNA BOROWIEC, MICHAŁ STANUSZEK

AGH University of Science and Technology

Abstract: Computer Aided Engineering (CAE) is commonly used in modern design of the various types of structures. There are two main issues/aspects that should be consider while using CAE in Geotechnics: the basic theory and material model. The paper deals with a problem of choosing the proper constitutive relationships which according to the authors are equally important in obtaining correct and reasonable results. This problem is illustrated by an example of dynamic calculations of fully saturated non-cohesive soils where liquefaction phenomenon is most likely to occur.

Key words: *liquefaction, constitutive relationships, UBC Sand model, Mohr–Coulomb model, numerical modeling in Plaxis*

1. INTRODUCTION

Dynamic excitations such as earthquakes, sea waves and currents are the main causes of the pore pressure build-up in the seabed soils. Excess pore pressure may pose a danger for the soil bearing capacity. If pore pressure is unable to dissipate on time the effective stress will decrease (according to Terzaghi's principle) and the soil skeleton will lose its shear strength (as the Coulomb criterion must be met). This phenomenon is known as the liquefaction.

The primary objective of this paper is to compare the well-known Mohr–Coulomb constitutive relationships with the relatively new and innovative UBC criterion, both implemented in the computational system called Plaxis 2D. The program mentioned is based on a finite element method and originates from Delft University of Technology (Netherlands). The revised version of Plaxis 2D – called Anniversary Edition (AE) will be used in calculations.

The UBC Sand model was introduced by Puebla et al. [10] in 1997, followed 13 years later by the extended 3-D version presented by Tsegaye [11]. In 2013, an improved model developed by Petalas [9] was presented together with a validation for different monotonic and cyclic stress paths. UBC criterion consists of a relatively simple but powerful approach in order to model the onset of the liquefaction phenomenon, which will be described later on.

The structure chosen for the calculation is a breakwater in Gdańsk's Northern Port, although it is the soil behavior that will be the most interesting. Three load sets are applied to the structure or to the seabed: an earthquake, waves acting on the breakwater and a combination of the two above occurring consecutively.

2. MATERIAL MODEL AND SOIL PARAMETERS

Geology of the subsoil (in seabed) is established on the basis of information obtained from [18]. Eastern part of breakwater in Gdansk's Northern Port rests on the gravel cushion, which is also introduced into the model. The seabed lays at a depth of 15 meters and is composed of two thick layers of sand divided by one thin layer of sandy silt/clay. Geometry of the model, soil layers, loads and sea level are all shown in Fig. 1.

UBC criterion as every advanced constitutive relationship needs some specific parameters which are

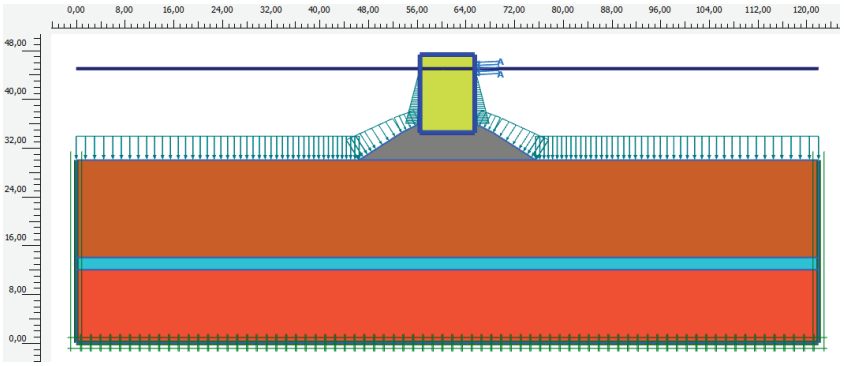

Fig. 1. Geometry of the Plaxis model

Table 1. Input parameters used in calculations

Parameter type	Material	Sand fill of breakwater	Gravel cushion	Sandy silt/clay	Sand (1)		Sand (2)		Break-water
	Color in the cross-sections in Fig. 1								
	Parameter \ Model	UBC MC	UBC MC	UBC MC	UBC	MC	UBC	MC	UBC MC
Basic	γ_{unsat} [kN/m^3]	18.0	19.0	18.0	19.7		19.7		n/a
	γ_{sat} [kN/m^3]	21.0	22.0	21.0	21.8		21.8		
	e_{init}	0.5	0.5	0.5	0.74		0.74		
	E [kPa]	83 330	225 000	11 140	98 000		98 000		
	ν	0.25	0.2	0.3	n/a	0.3	n/a	0,3	
	G [kPa]	33 330	93 750	4 286		28 000		28 000	
	c_{ref} [kPa]	5.0	5.0	60.0	0.0		0.0		
	φ [°]	35.0	40.0	33.0	22.0		22.0		
	ψ [°]	0.0	0.0	0.0	19.0		18.0		
	k_x, k_y [m/s]	2.2e-3	5.0e-3	0.5e-7	0.5e-6		2.0e-6		
Constitutive model	φ_{cv} [°]	n/a	n/a	n/a	20.0	n/a	20.0	n/a	n/a
	φ_p [°]				22.0		23.0		
	K_G^e				854.6		954.1		
	K_G^p				250.0		424.7		
	K_B^e				598.2		667.9		
	me				0.5		0.5		
	ne				0.5		0.5		
	np				0.5		0.5		
	R_f				0.811		0.771		
	P_A [kPa]				100.0		100.0		
	σ_t [kPa]				0.0		0.0		
	fac_{hard}				0.2		0.2		
	$(N1)_{60}$				7.65		10.65		
	fac_{post}				0.02		0.02		
Rigid body	EA_1 [kN/m]	n/a	n/a	n/a	n/a		n/a		12.0e6
	EA_2 [kN/m]								12.0e6
	EI [kPa/m]								160.0e3
	d [m]								0.4
	w [kN/m/m]								20.0

obtained mainly from laboratory tests. For the purpose of those calculations they are established following the example included in [2]. In the case of the Mohr–Coulomb (MC) criterion, parameters are set on the basis of the soil classification proposed by [12]. All input parameters concerning soil, constitutive relationship and breakwater are gathered in Table 1.

The UBC material model "utilizes isotropic and simplified kinematic hardening rule for primary and secondary yield surfaces, in order to take into account

the effect of soil densification and predict a smooth transition into the liquefied state during undrained cyclic loading. By means of a simplified Rowe stress dilatancy theory the model is capable of modeling cyclic liquefaction for different stress paths. Post liquefaction behavior of loose sands and cyclic mobility of dense sands can be modeled in terms of a stiffness degradation rule." [9]

The input parameters of the UBC material model, their significance and the methods of establishing are summarized in Table 2.

Using different combinations of calculation phases six numerical models are created in total (see Table 3), three for UBC criterion and the another three for the Mohr–Coulomb (MC). The main purpose here is to see how the subsoil behavior changes (especially pore pressure) for both of these criterions under tree different dynamic excitations: earthquake motion, sea wave loading and the sea waves coming on the structure just after the earthquake has ceased. Phase called *Initial* (Phase 0) serves to determine Initial Stresses and hydrostatic field of pore water pressure. Like in every geotechnical program using numerical methods, this phase is obligatory and cannot be deactivated. Secondary the consolidation which always precedes the remaining dynamic phases is conducted and it lasts 30 days.

The earthquake used in calculations is acquired from [17] and chosen as the most relevant and similar

Table 2. The meaning of input parameters used in material model

Name	Symbol	Establishing method
Constant volume friction angle	φ_{cv}	CD Triaxial Test or Direct Simple Shear
Peak friction angle	φ_p	
Elastic Bulk Modulus	K_B^e	Drained Triaxial Test with a confining pressure of 100 kPa.
Elastic Shear Modulus	K_G^e	Related with the K_B^e using the Poison ratio
Plastic shear modulus	K_G^p	Extracted after curve fit
Elastic Bulk Modulus Index	*me*	
Elastic Shear Modulus Index	*ne*	
Plastic Shear Modulus Index	*np*	
Failure Ratio	R_f	
Densification factor (a multiplier that controls the scaling of the plastic shear modulus during secondary loading)	fac_{hard}	
Post Liquefaction Factor	fac_{post}	
Corrected SPT value	$(N1)_{60}$	*In situ* testing
Tension cut-off	σ_t	–

Table 3. Phases for all numerical models

Model	UBC-1	UBC-2	UBC-3	MC-1	MC-2	MC-3
Applied type of load	Only earthquake	Only sea waves	Both earthquake & sea waves	Only earthquake	Only sea waves	Both earthquake & sea waves
Phase 0	Static: Initial					
Phase 1	Static: Consolidation [30 days]					
Phase 2	Dynamics: earthquake [80 sec]	Cyclic: first sea wave [5 sec]	Dynamics: earthquake [80 sec]	Dynamics: earthquake [80 sec]	Cyclic: first sea wave [5 sec]	Dynamics: earthquake [80 sec]
Phase 3	n/a	Cyclic: second sea wave [5 sec]	Static: Plasticity	n/a	Cyclic: second sea wave [5 sec]	Static: Plasticity
Phase 4		Cyclic: third sea wave [5 sec]	Cyclic: first sea wave [5 sec]		Cyclic: third sea wave [5 sec]	Cyclic: first sea wave [5 sec]
Phase 5		n/a	Cyclic: second sea wave [5 sec]		n/a	Cyclic: second sea wave [5 sec]
Phase 6			Cyclic: third sea wave [5 sec]			Cyclic: third sea wave [5 sec]

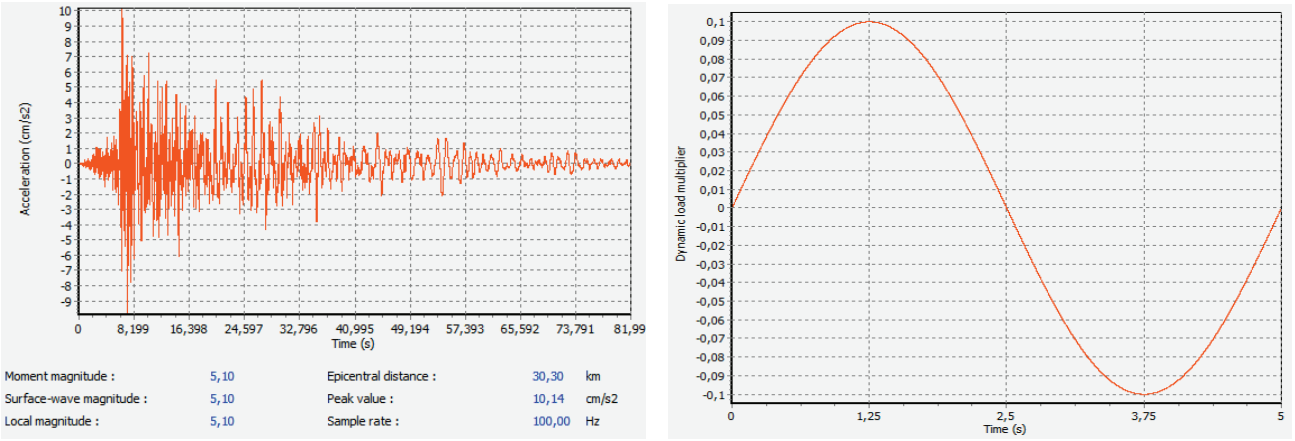

(a) (b)

Fig. 2. Dynamic loading: (a) the record of earthquake accelerations, (b) sea waves function

to ones observed in Northern Poland and the Baltic Sea Region. The record of earthquake accelerations, along with its magnitude of 5.10 (in the open-ended Richter scale) and peak value of 10.14 cm/s^2 is shown in Fig. 2a. Earthquake accelerations are submitted to the base of the model. Figure 2b presents the sea wave load, which is applied as a sinusoidal function with the amplitude of 0.1 m and frequency of 0.2 Hz, to the upper part of breakwater wall over a height of 2.0 meters (see Fig. 1).

3. RESULTS OF CALCULATIONS

According to the Finite Element Method a continuum is divided into a finite number of elements to give a discrete mesh. Each element consists of a specific amount of nodes which provide degrees of freedom corresponding to the unknowns in the problem. Plaxis 2D is based on Biot's theory of dynamic consolidation where at every node there is a vector of displacements and a scalar of pore pressure. In this example the mesh is generated using fifteen-node triangular elements giving the total number of Fes a little over 1100. Since the mesh density plays lesser part in the dynamic analysis (as long as the Nyquist condition is fulfilled), the mesh was optimized to save calculation time [3].

In such complex analysis not only material parameters (mentioned before) but also factors of numerical procedure must be selected with full awareness and care. For example, in the UBC-2 and UBC-3 model, the wave load generates an excessive displacements and disturbs results coming from previous construction phases. The problem can be solved by reducing and controlling so called *prescribed displacement resulting from earthquakes*.

Figures included in the paper present if not stated otherwise, the results after the last phase of calculations.

3.1. DISPLACEMENTS AND STRAINS

Maximum values of computed displacements are located (as expected) just beneath the breakwater. They are presented in Table 4 and it is easy to observe that they are at least two orders of magnitude smaller in the MC than in UBC models. Therefore, it is clear that subsoil modeled by means of UBC criterion, tends to liquefy while seabed in all MC model shows no signs of liquefaction. It is also worth mentioning that in the UBC-1 model the gravel cushion behaves like a rigid body and *sinks* into lose sands of the seabed – typical behavior confirmed not only by several laboratory simulations but also observed during or after real earthquakes.

Table 4. Summary of maximum displacements

Model UBC		Model MC	
No.	Total displacements [m]		No.
1	0.41	$3{,}28 \cdot 10^{-3}$	1
2	14.29	$0{,}37 \cdot 10^{-3}$	2
3	0.15	$3{,}14 \cdot 10^{-3}$	3

Displacements exceeding 14.0 m are of major concern. They are obtained in UBC-2 model although after passage of the first sea wave they were reaching only 10 cm. Their increase with each subsequent wave eventually gives the value of 14 meters (see Fig. 3). To improve the situation different possibilities were

examined. First the load was applied to the seabed, then to entire structure (i.e., breakwater and gravel cushion) and finally to both of them. Unfortunately, regardless of where and how the sea waves were applied, displacements still accumulated achieving unrealistic values. Also the attempts to change load amplitude and its frequency did not improve the situation significantly. Thus the UBC-2 model is either extremely prone to the liquefaction or completely unstable under this specific type of cyclic loading.

In the case of analogical model for the Mohr–Coulomb criterion (MC-2) similar problem does not occur and total displacements are reasonable. In that content the Mohr–Coulomb constitutive relationship seams to be more suitable for modeling soil behavior subjected to the motions of the sea. At the same time all MC models allow for the static forces to prevail and extreme displacements to form a classical slip plane, visible on the example of MC-1 displacements in Fig. 4.

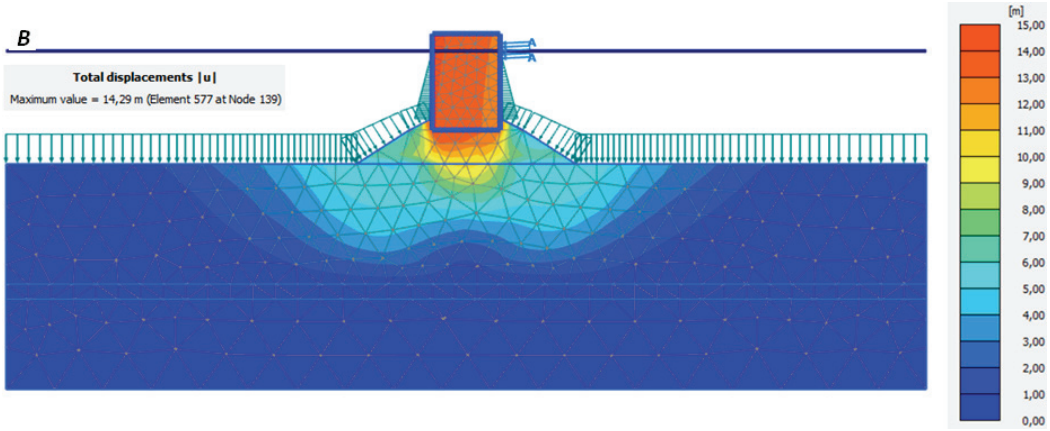

Fig. 3. Total displacements for UBC-2 model

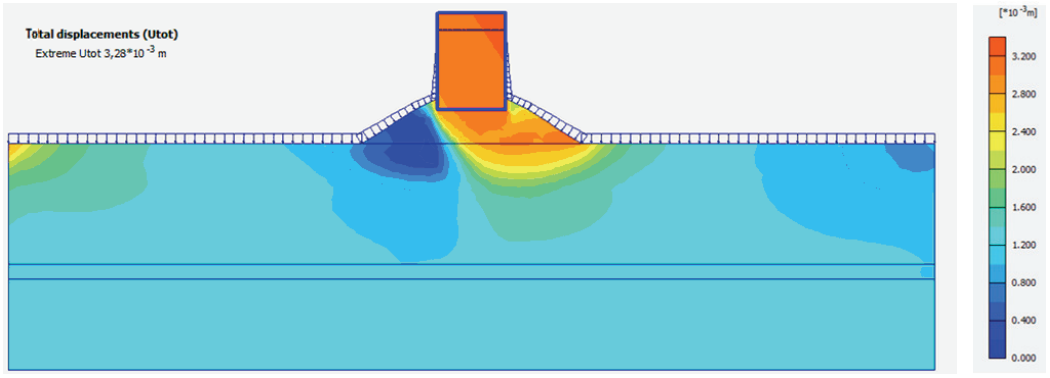

Fig. 4. Total displacements for MC-1 model

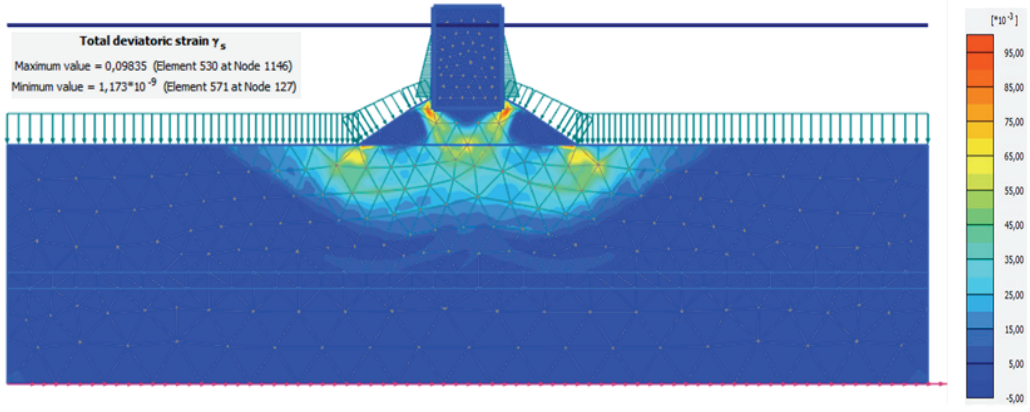

Fig. 5. Deviatoric strain distribution for UBC-1 model

Plaxis 2D allows different components of strain tensor to be calculated, but most interesting from the mechanical point of view are volumetric and deviatoric ones. In both MC and UBC models they attain very low values and concentrate close to the corners of the breakwater and gravel cushion (see Fig. 5).

3.2. STRESS DISTRIBUTIONS

Plaxis postprocessor called *Output* offers a wide range of results also for the stress tensor, among them: total, effective, hydrostatic, deviatoric, normal, shear and principal stresses. Extreme values of stress of the greatest importance for the analysis are shown in Table 5.

Regardless of the load type (static, cyclic or dynamic) the shear stress distributions for all models using the Mohr–Coulomb criterion appear to be almost identical (see Fig. 6). The main influence on effective stresses has therefore a dead load and hydrostatic pressure, not the dynamic excitation. That proves once again how poorly the Mohr–Coulomb constitutive relationship manages with liquefaction phenomenon.

Table 5. Summary of extreme stress values

Model UBC	Model MC	
No.	Shear stresses σ_{xy} [kPa]	No.
1	178.8	–84.36	1
2	–180.9	–82.81	2
3	–173.6	–84.34	3
	Hydrostatic stresses σ_{hydr} [kPa]	
1	–646.7	–361.62	1
2	–517.7	–361.65	2
3	–413.7	–361.64	3
	Deviatoric stresses σ_{dev} [kPa]	
1	406.7	317.5	1
2	406.1	317.5	2
3	367.4	317.2	3

The alternate material model, called UBC Sand, proposed in the paper gives better results, as expected. Although the extreme values of shear stresses for these models are similar, their distributions differ significantly (see Fig. 7). Firstly they are no longer symmetrical and secondly much more difficult to assess.

In order to follow more accurate results especially in time domain some curves are generated at the most strategic points of the geometry. Figure 8 shows the location of the cross sections and points chosen to visualize the time-dependent results.

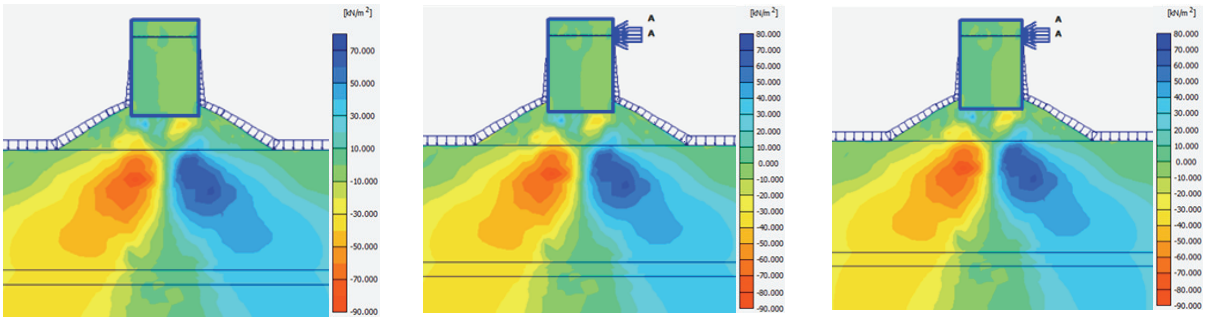

a) b) c)

Fig. 6. Shear stress distribution in the central part of: (a) MC-1 model, (b) MC-2 model, (c) MC-3 model

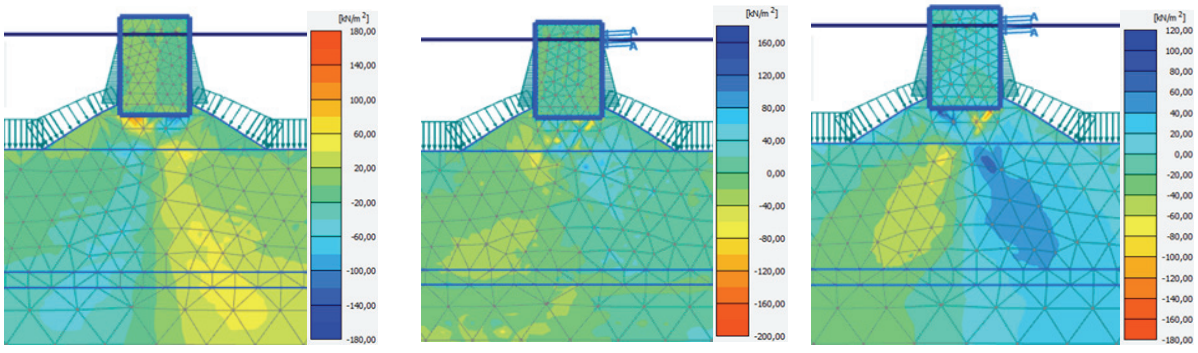

a) b) c)

Fig. 7. Shear stress distribution in the central part of: (a) UBC-1 model, (b) UBC-2 model, (c) UBC-3 model

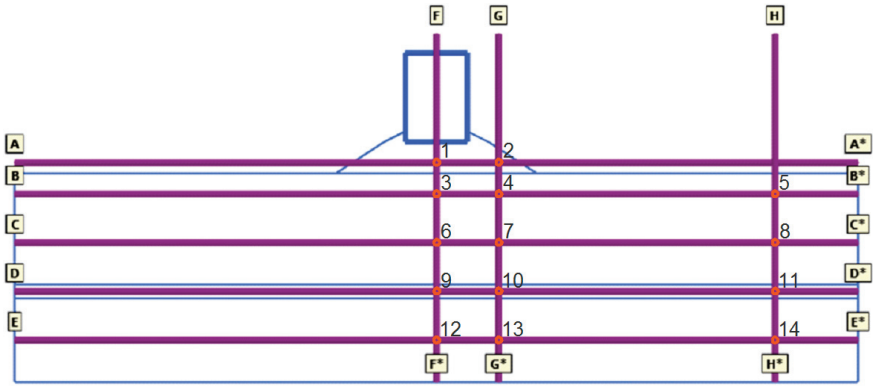

Fig. 8. Cross-sections and points chosen for graphs

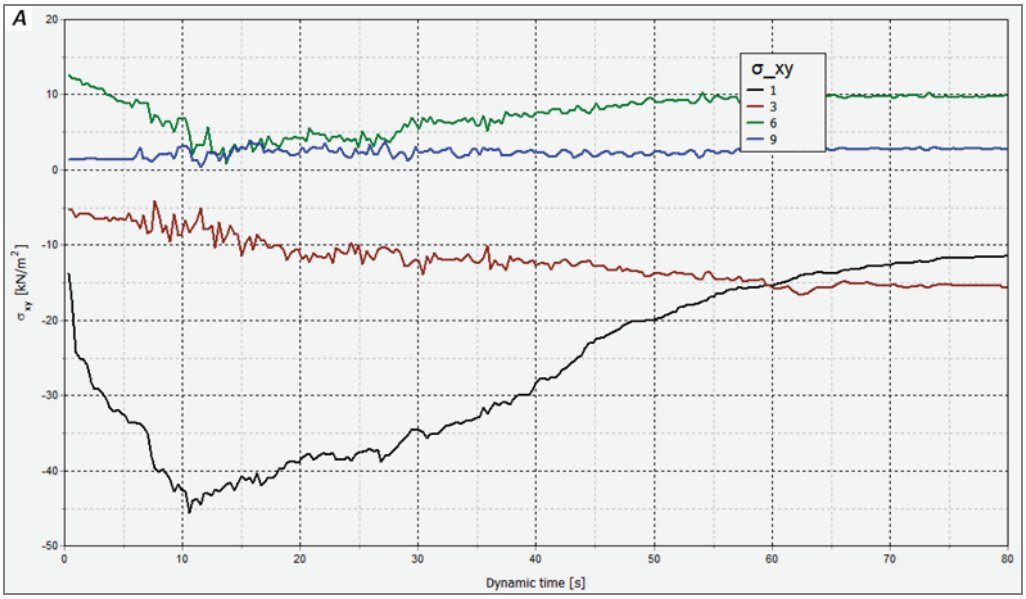

Fig. 9. UBC-1 model: Shear stresses varying with time at four points along the F-F* cross-section

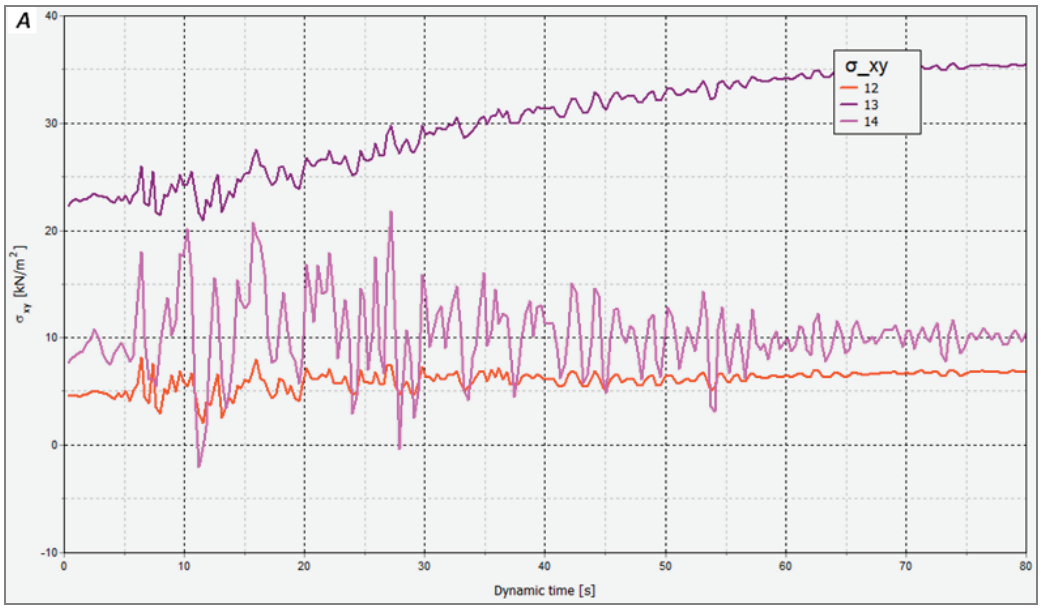

Fig. 10. UBC-1 model: Shear stresses varying with time at three points along the E-E* cross-section

Curves in Fig. 9 are generated for the UBC-1 model at four points along the F-F cross-section. Shear stress variations with time show not only some oscillations (dynamic response) but also visible drops. These minima are reached in the 10th second of excitation approximately. In respect of the subsoil shear strength this moment of the earthquake can be called critical. It is also the most probable moment for the liquefaction onset.

Figure 9 illustrates also how the reaction to the loading changes for different materials. The point inside the gravel cushion (curves No. 1 in Fig. 9) shows the strongest response to the dynamic excitation – sign of elastic rather than plastic behavior. The opposite reaction (or no reaction at all) is demonstrated by the thin layer of sandy silt/clay (curves No. 9 in Fig. 9). Thus UBC model during dynamic calculation can most properly distinguish between cohesive and loose material.

Although points for curves in Fig. 10 are picked from one soil layer they indicate quite anisotropic response, differing not only in respect of amplitude but also tendency. This phenomenon is typical of dynamic problems where geometry of the structure (here the lay-out of soil deposits) plays the dominant role. Shear waves do not propagate in any symmetric manner and may be amplified by waves reflected from the boundary of two different soil layers (boundary of materials with two different densities precisely). In Fig. 9 and Fig. 10, an attenuation and damping can also be observed.

3.3. EXCESS PORE PRESSURE

Excess pore pressure is a rapid increase in pore pressures caused by the extremely quick application of loading and unloading, which cannot be dissipated. The accumulation of excess pore pressure is a first sign of liquefaction. According to Biot's theory of dynamic consolidation, which is implemented in Plaxis 2D, this phenomenon should take place during dynamic phase of calculations. As shown in Table 6, all models with the Mohr–Coulomb criterion do not demonstrate any significant growth in pore pressures. This means that it is not only the theory on which the program is based, but also available material models that matters the most.

Table 6. Values of extreme excess pore pressure

Model UBC		Model MC
No.	Excess pore pressure [kPa]	No.
1	700.7	33.10	1
2	424.1	29.46	2
3	1296	33.68	3

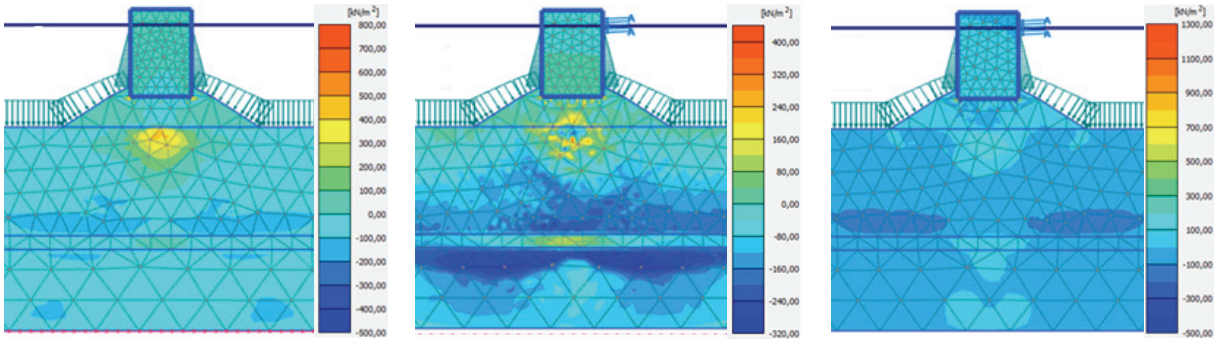

a) b) c)

Fig. 11. Excess pore pressure in the central part of: (a) UBC-1 model, (b) UBC-2 model, (c) UBC-3 model

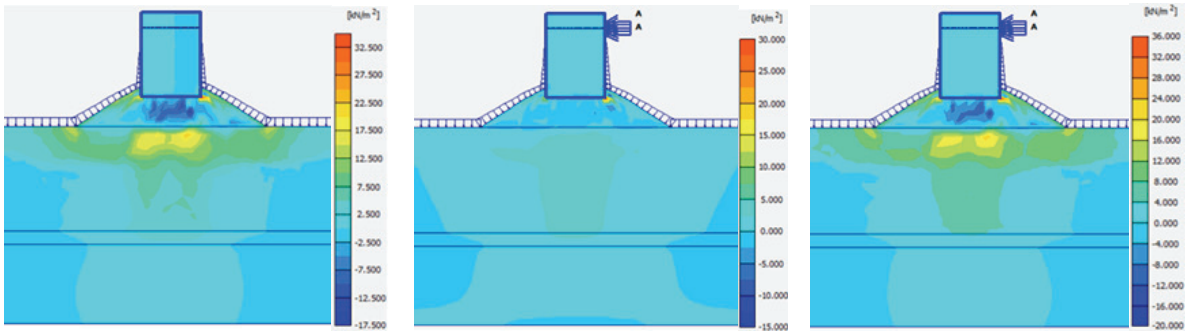

a) b) c)

Fig. 12. Excess pore pressure in the central part of: (a) MC-1 model, (b) MC-2 model, (c) MC-3 model

Drainage of water from the seabed during unloading causes suction in its deeper regions. This is particularly apparent in the UBC-2 model in Fig. 11b. Area of negative excess pore pressure is separated by less permeable layer of sandy silt/clay that restricts filtration of the water and thus dissipation of pore pressure.

Excess pore pressure distribution in UBC models (see Fig. 11) is much more realistic than in MC models. Extreme values for UBC are at least ten times higher than for MC models (Table 6). The seabed consists mostly of the loose materials in which drained conditions prevail and pore pressure build-up is very unlikely. It is completely understandable in so called static consolidation but should not take place in dynamic analysis. Fully saturated loose materials during dynamic consolidation tend to liquefy – the first symptom of what is a growth in pore pressure. For all MC models, as shown in Fig. 12, excess pore pressure cumulates right below the gravel cushion but does not exceed the value of 30 kPa and dissipates in the layer of sand lying below. In the same phase of calculation for UBC models (see Fig. 11) large concentrations of pore pressure (with extreme values up to 1296 kPa) can be observed in several parts of soil layers, i.e., first locations to liquefy.

The diagrams in Fig. 13 present the excess pore pressure changes with time, which appear to be almost constant until the 10th second of the excitation, and which then begin to demonstrate irregular and oscillatory characteristic. The same critical time can be observed for some shear stresses in Fig. 9. It obviously corresponds to the time when the peak value of the accelerations occurs during earthquake (see Fig. 2a). Although this reaction cannot be detected in the entire geometry, it is mostly visible directly below the breakwater (curves No. 3 in Fig. 13).

3.4. VOID RATIO

At the end of all construction phases void ratio slightly differs from its initial values (Table 1). Shown in Fig. 14 the final void ratio distribution can be still quite useful to trace how the body waves propagate in porous media or which parts of the subsoil (built with loose materials) can be compacted most easily.

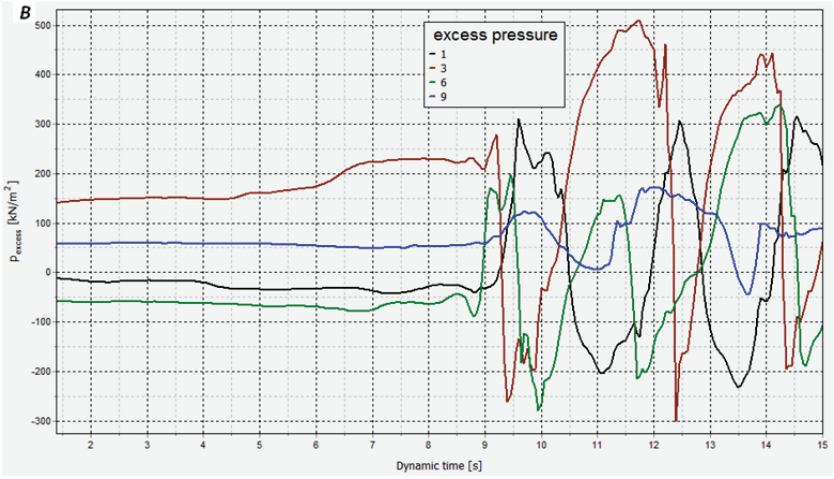

Fig. 13. UBC-2 model: Excess pore pressure diagram with respect to time at four points along the F-F*

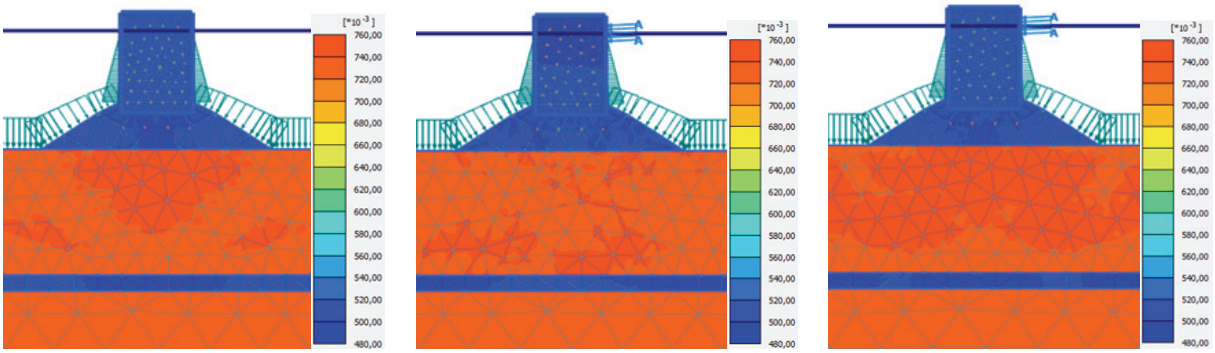

a) b) c)

Fig. 14. Void ratio in the central part of: (a) UBC-1 model, (b) UBC-2 model, (c) UBC-3 model

3.5. MOBILIZED SHEAR STRENGTH

In soil mechanics failure occurs when the shear stresses exceed the material shear strength. Mobilized shear strength is a resistance of soil which arises against tangential stress along the slip surface. Figure 15 shows the mobilized shear strength for UBC models, which demonstrate not only the high values but also remarkable distribution. Extreme values of mobilized shear strength form a shape similar to the vertical pylon or cone, stretching from the base of breakwater to the base of the model, indicating the most resistant parts of the subsoil.

On the other hand, the Mohr–Coulomb constitutive relationship seams to be more suitable for modeling soil behavior subjected to the motions of the sea – here models using UBC criterion showed some inconsistency. Especially in UBC-2 model, where displacements were several times larger than in the two remaining models and where the subsoil stability was hard to achieve. UBC-2 model had first two construction phases the same as UBC-1 model but was not providing the matching results as long as *prescribed displacements resulting from earthquakes* were changed, although it seems to be rather technical than substantive problem.

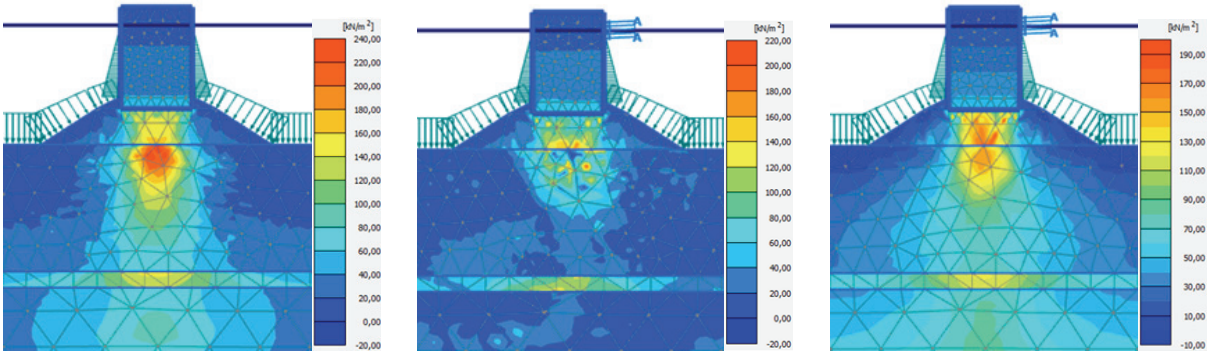

a) b) c)

Fig. 15. Mobilized shear strength in the central part of: (a) UBC-1 model, (b) UBC-2 model, (c) UBC-3 model

4. SUMMARY

Plaxis AE is a sophisticated calculation system whose possibilities and wide range of output data are demonstrated in this paper.

For models using the Mohr–Coulomb constitutive relationship, regardless of the type of dynamic loading pore pressures and shear stresses do not differ significantly. There is no indication of any failure during or after dynamic excitation and overall stability of these models is preserved. They are also unable to demonstrate the excess of the pore pressure induced by dynamic excitation. Build-up of pore pressure occurs only in cohesive soils during consolidation phase. Thus MC models are unable to distinguish between static and dynamic consolidation. Dead load and hydrostatic pressure have the main influence on the soil behavior here. Summing up, calculations performed for the purpose of this paper confirmed that the Mohr–Coulomb constitutive relationship is unable to model liquefaction phenomenon properly.

In the content of the whole calculations UBC-1 (where from dynamic loads only earthquake was applied) seemed to be the most reliable liquefaction model.

It was also demonstrated that either in dynamic or static consolidation the results (especially pore pressures and shear stresses) should be observed not only in space but also in time domain: in the case of static consolidation to indicate the end of consolidation process and in the case of dynamic consolidation to catch the most probable moment of the liquefaction onset.

The complexity of the liquefaction phenomenon forces engineers working with such advanced programs as Plaxis AE to take particular care while interpreting the results and using them in design. The purpose of the article was also to draw attention to the fact that in more general content in Computer Aided Engineering (CAE) not only the theory standing behind the governing equations but also constitutive relationship would influence the results the most and in the extreme case would not allow the possible failure to be recognized.

REFERENCES

[1] CHEN J.W., CHEN F.C., *The penetration experiment to predict liquefaction resistance of reclaimed soils*, Ocean Engineering, 2008, 35, 380–392.

[2] DAFTARI A., KUDLA W., *Prediction of Soil Liquefaction by Using UBC3D-PLM Model in PLAXIS*, International Journal of Environmental, Ecological, Geological and Mining Engineering, 2014.

[3] GALAVI V. et al., *Finite Element Modelling of Seismic Liquefaction in Soils*, Geotechnical Engineering Journal of the SEAGS & AGSSEA, 2013, 44.

[4] HARITOS N., *Modelling ocean waves and their effects on offshore structures*, Australian Earthquake Engineering Society 2010 Conference.

[5] HWANG J.H. et al., *A practical reliability-based method for assessing soil liquefaction potential*, Soil Dynamics and Earthquake Engineering, 2004, 24, 761–770.

[6] NOORZAD R. et. al., *The effect of structures on the wave-induced liquefaction potential of seabed sand deposits*, Applied Ocean Research, 2009, 31, 25–30.

[7] MAKRA A., *Evaluation of the UBC3D-PLM constitutive model for prediction of earthquake induced liquefaction on embankment dams*, MSc. Graduation Thesis, 2013.

[8] LENZ A., BAISE G., *Spatial variability of liquefaction potential in regional mapping using CPT and SPT data*. Soil Dynamics and Earthquake Engineering, 2007, 27, 690–702.

[9] PETALAS A., GALAVI V., *Plaxis Liquefaction Model UBC3D-PLM*, PLAXIS, 2013.

[10] PUEBLA H., BYRNE M., PHILLIPS P., *Analysis of CANLEX liquefaction embankments prototype and centrifuge models*,. Canadian Geotechnical Journal, 1997, 34, 641.

[11] TSEGAYE A.B., *Liquefaction Model UBC3D*, PLAXIS, 2010.

[12] WIŁUN Z., *Zarys geotechniki*, Wydawnictwo Komunikacji i Łączności, 2013.

[13] WINTERWERP J.C. et al., *Mud-induced wave damping and wave-induced liquefaction*, Coastal Engineering, 2012, 64, 102–112.

[14] XIAO H. et al., *Parametric study of breaking solitary wave induced liquefaction of coastal sandy slopes*, Ocean Engineering, 2010, 37, 1546–1553.

[15] YE. J., *3D liquefaction criteria for seabed considering the cohesion and friction of soil*, Applied Ocean Research, 2012, 37, 111–119.

[16] ZHANG Y. et al., *An analytical solution for response of a porous seabed to combined wave and current loading*, Ocean Engineering, 57, 240–247, 2013.

[17] Strong-Motion Virtual Data Center, Center for Engineering Strong Motion Data, strongmotioncenter.org

[18] Central Geological Database, Polish Geological Institute, m.bazagis.pgi.gov.pl

[19] COSMOS Virtual Data Center, Consortium of Organizations for Strong-Motion Observation Systems, cosmos-eq.org